

## Interaction between Turbulence and Neoclassical Dynamics and Its Effect on Tokamak Transport: Gyrokinetic Simulations and Theory

W. X. Wang 1), T. S. Hahm 1), S. Ethier 1), G. Rewoldt 1), W. W. Lee 1), W. M. Tang 1), S. M. Kaye 1), P. H. Diamond 2)

1) Princeton Plasma Physics Laboratory, P. O. Box 451, Princeton, New Jersey 08543, USA

2) University of California, San Diego, California 92093, USA

wwang@pppl.gov

**Abstract.** The relationship between momentum and energy transport is investigated with focus on understanding recent experimental observations, using global gyrokinetic simulations with proper coupling between turbulence and neoclassical dynamics. First, a large inward flux of toroidal momentum is found robustly in the post saturation phase of ion temperature gradient (ITG) turbulence. As a consequence, core plasma rotation spins up. The underlying physics for the inward flux is identified to be the generation of residual stress due to the  $k_{\parallel}$  symmetry breaking induced by self-generated zonal flow shear which is rather stationary in global simulations. Our neoclassical simulations have observed an enhancement of neoclassical momentum transport in steep rotation gradient regions and a significant inward nondiffusive momentum flux driven by ion temperature gradients. However, the overall neoclassical contribution to the toroidal momentum transport is negligibly small. It is found that residual turbulence can survive the dissipation of a strong mean  $\mathbf{E} \times \mathbf{B}$  flow shear and drive a significant momentum flux. Moreover, the equilibrium  $\mathbf{E} \times \mathbf{B}$  flow shear is found to reduce the turbulence driven transport for energy more efficiently than for momentum. These findings may offer one explanation for recent puzzling experimental observations that the toroidal momentum transport remains highly anomalous, even while the ion heat flux is reduced to a neoclassical level.

### I. Introduction

The  $\mathbf{E} \times \mathbf{B}$  flow shear is well known to reduce low-k turbulence and associated anomalous transport, in particular, the ion heat flux. Via the radial force balance, the equilibrium  $\mathbf{E} \times \mathbf{B}$  flow is related to the plasma pressure profile and rotations which, in turn, are governed by energy, particle and momentum transport. Recent studies of momentum transport in toroidal systems have been motivated by attempts to understand the spontaneous or intrinsic rotation discovered in experiments.<sup>1</sup> There has been increased research interest in this aspect, focusing on searching for and understanding non-diffusive mechanisms. Global gyrokinetic simulations using the Gyrokinetic Tokamak Simulation (GTS) code<sup>2</sup> have been carried out to investigate turbulence driven momentum and energy transport and their relationship for realistic tokamak parameters. Moreover, recent findings from experiments indicate that the toroidal momentum transport remains highly anomalous, even while the ion heat flux is reduced to a neoclassical level,<sup>3</sup> presumably due to the suppression of low-k turbulence in the presence of strong  $\mathbf{E} \times \mathbf{B}$  shear. Motivated by this observation, we investigate the possibility that some residual low-k turbulence, even in the presence of relatively strong  $\mathbf{E} \times \mathbf{B}$  shear, can lead to a momentum flux level much higher than the neoclassical value, but with ion heat flux on the order of the neoclassical value. This issue is also highly relevant to ITER because similar phenomena may occur in transport barriers of burning plasmas where stabilization of resistive wall modes relies on the rotation.

GTS simulation is based on a generalized gyrokinetic simulation model with a particle-in-cell approach, and incorporates the comprehensive influence of non-circular cross section, realistic

plasma profiles, plasma rotation, neoclassical (equilibrium) electric field, Coulomb collisions, and other features. It directly reads plasma profiles of temperature, density and toroidal angular velocity, from the TRANSP experimental database, and a numerical MHD equilibrium reconstructed by the JSOLVER or ESC code using TRANSP radial profiles of the total pressure and the parallel current (or safety factor), along with the plasma boundary shape. Also studied are the counterparts of neoclassical transport using the GTC-NEO code.<sup>4</sup>

## II. Gyrokinetic simulation model for rotating plasma and turbulence dynamics

The gyrokinetic simulation model for rotating plasmas is briefly described first. The gyrokinetic particle distribution is expressed as  $f = f_0 + \delta f$ . Here we separate the turbulence perturbation  $\delta f$  from the equilibrium distribution  $f_0$ . The equilibrium distribution function  $f_0$ , with magnetic moment  $\mu$  and parallel velocity  $v_{\parallel}$  as independent velocity variables, is determined by the neoclassical dynamics and obeys

$$\frac{\partial f_0}{\partial t} + (v_{\parallel} \hat{\mathbf{b}} + v_{E_0} \vec{v} + v_d \vec{v}) \cdot \nabla f_0 - \hat{\mathbf{b}}^* \cdot \nabla (\mu B + \frac{e}{m_i} \Phi_0) \frac{\partial f_0}{\partial v_{\parallel}} = C_i(f_0, f_0). \quad (1)$$

Here  $v_{E_0}$  is the  $\mathbf{E} \times \mathbf{B}$  drift velocity corresponding to the equilibrium potential  $\Phi_0$ .  $v_d$  is the  $\nabla B$  drift velocity,  $\hat{\mathbf{b}}^* = \hat{\mathbf{b}} + \rho_{\parallel} \hat{\mathbf{b}} \times (\hat{\mathbf{b}} \cdot \nabla \hat{\mathbf{b}})$  with  $\hat{\mathbf{b}} = \mathbf{B}/B$ , and  $C_i$  is the Coulomb collision operator. The lowest order solution of Eq. 1 is a shifted Maxwellian consistent with (large) plasma rotation:<sup>4</sup>

$$f_0 = f_{SM} = n(r, \theta) \left( \frac{m_i}{2\pi T_i} \right)^{3/2} e^{-\frac{m_i}{T_i} [\frac{1}{2}(v_{\parallel} - U_i)^2 + \mu B]}, \quad (2)$$

where the parallel flow velocity  $U_i$  is associated with the toroidal rotation by  $U_i = I\omega_t/B$  with  $\omega_t$  the toroidal angular velocity and  $I$  the toroidal current, and  $n(r, \theta)$  is the ion density  $n(r, \theta) = N(r) e^{\frac{m_i U_i^2}{2T_i} - \frac{e\tilde{\Phi}_0}{T_i}}$ . The total equilibrium potential consists of two parts,  $\Phi_0 = \langle \Phi_0 \rangle + \tilde{\Phi}_0$ . Here,  $\langle \rangle$  denotes a flux surface average. The poloidally varying component  $\tilde{\Phi}_0$  can be generated by the centrifugal force which drives charge separation on a magnetic surface in strongly rotating plasmas.<sup>5</sup> Generally the radial potential  $\langle \Phi_0 \rangle$  is dominant. The equilibrium radial electric field can be calculated from a first-principles based particle simulation of neoclassical dynamics with important finite orbit effects,<sup>4</sup> or obtained by direct experimental measurement if available. Instead of using a true neoclassical equilibrium distribution function, which is unknown analytically, we use this lowest order solution for equilibrium toroidal plasmas. A shifted Maxwellian with either model or experimental profiles of  $\langle n(r, \theta) \rangle$ ,  $T_i(r)$  and  $\omega_t(r)$  is prescribed for the ions. In the electrostatic limit, the ion gyrokinetic equation for the turbulence perturbation  $\delta f_i$  is

$$\begin{aligned} & \frac{\partial \delta f_i}{\partial t} + (v_{\parallel} \hat{\mathbf{b}} + v_{E_0} \vec{v} + v_E \vec{v} + v_d \vec{v}) \cdot \nabla \delta f_i - \hat{\mathbf{b}}^* \cdot \nabla (\mu B + \frac{e}{m_i} \Phi_0 + \frac{e}{m_i} \bar{\Phi}) \frac{\partial \delta f_i}{\partial v_{\parallel}} \\ & = \left\{ - \left[ \frac{m}{T_i} \left( \frac{1}{2}(v_{\parallel} - U_i)^2 + \mu B \right) - \frac{3}{2} \right] v_E \vec{v} \cdot \nabla \ln T - v_E \vec{v} \cdot \nabla \ln n(r, \theta) \right. \\ & \quad \left. - \frac{m(v_{\parallel} - U_i)}{T_i} v_E \vec{v} \cdot \nabla U_i(r, \theta) + \frac{m U_i}{T_i v_{\parallel}} v_E \vec{v} \cdot \mu \nabla B - \frac{1}{T_i} (v_{\parallel} \hat{\mathbf{b}} + v_d \vec{v}) \cdot \nabla (e\bar{\Phi}) \left( 1 - \frac{U_i}{v_{\parallel}} \right) \right\} f_0. \quad (3) \end{aligned}$$

Here  $v_E$  is the  $\mathbf{E} \times \mathbf{B}$  velocity corresponding to the fluctuation potential  $\bar{\Phi}$ , and  $C_i^l$  is the linearized Coulomb collision operator. On the right hand side, the third term proportional to  $\nabla U_i$  is the Kelvin-Helmholtz-type driver term, The other terms containing  $U_i$  are also retained, which can be important when the Mach number of plasma flow is high.

Global gyrokinetic turbulence is characterized by distinguishable dynamical phases, from linear, to nonlinear transient, to a well developed turbulent state. In coordinate space, toroidal eigenmodes are driven initially in the linearly unstable region, forming radially elongated streamers.

Later on, the streamers are broken by the self-generated zonal flow during nonlinear saturation. A major turbulence radial spreading associated with nonlinear wave coupling immediately follows, resulting in global turbulence.<sup>2</sup> In wavenumber space, after the linear growth of instability, nonlinear toroidal couplings transfer energy from the linearly unstable modes to longer wavelength damped modes, and form a down-shifted toroidal spectrum in the fully developed turbulence regime.<sup>6</sup>

Ideally, the dynamics of gyrokinetic turbulence should not be sensitive to numerical techniques. This has been carefully examined for GTS simulations. The GTS code solves the gyrokinetic Poisson equation in coordinate space, and in simulations it, in principle, retains all (m,n) modes from (0,0) all the way to a limit which is set by grid resolution, and therefore retains complete nonlinear energy coupling channels. There are two largely different Poisson solvers implemented in the GTS simulation. In a simple geometry limit, i.e, large aspect ratio and circular cross section, turbulence fluctuations  $\delta\Phi$  on small spatial and fast time scales and axisymmetric zonal flow  $\langle\Phi\rangle$  on large spatial and slow time scales can be decoupled using i) a Pade approximation, i.e,  $\Gamma_0(b) \equiv I_0(b)e^{-b} \approx 1/(1+b)$  with  $I_0$  the modified Bessel function and  $b = (k_\perp \rho_i)^2$ , and ii)  $\langle\tilde{\Phi}\rangle \approx \langle\Phi\rangle$ . The resulting two equations are<sup>2</sup>

$$\left(1 + \frac{T_i}{T_e}\right) \frac{e\delta\Phi}{T_i} - \frac{e\tilde{\delta\Phi}}{T_i} = \frac{\delta\bar{n}_i - \langle\delta\bar{n}_i\rangle}{n_0} - \frac{\delta n_e^{(1)} - \langle\delta n_e^{(1)}\rangle}{n_0}, \quad (4)$$

$$\begin{aligned} \frac{1}{\mathcal{V}'_r} \frac{d}{dr} \left[ \frac{d\Phi_{00}}{dr} \mathcal{V}'_r \langle g^{rr} \rangle \right] &= \frac{1}{\mathcal{V}'_r} \frac{d}{dr} \left\{ \frac{d}{dr} \left[ \frac{T_i}{e} \left( \frac{\langle\delta\bar{n}_i\rangle}{n_0} - \frac{\langle\delta n_e^{(1)}\rangle}{n_0} \right) \right] \mathcal{V}'_r \langle g^{rr} \rangle \right\} \\ &\quad - \left\langle \frac{1}{\rho_i^2} \right\rangle \frac{T_i}{e} \left( \frac{\langle\delta\bar{n}_i\rangle}{n_0} - \frac{\langle\delta n_e^{(1)}\rangle}{n_0} \right). \end{aligned} \quad (5)$$

Because turbulence dynamics on different spatio-temporal scales are separated in solving the Poisson equation, the advantages are apparent. However, the above approximations, particular the second one, are not justified in general toroidal geometry. This has motivated us to develop a generalized Poisson solver which solves an integral equation for the total potential:  $\Phi = \delta\Phi + \langle\Phi\rangle$ ,

$$\left(1 + \frac{T_i}{T_e}\right) \frac{e\Phi}{T_i} - \frac{e\tilde{\Phi}}{T_i} - \frac{e\langle\Phi\rangle}{T_e} = \frac{\delta\bar{n}_i}{n_0} - \frac{\delta n_e^{(1)}}{n_0}. \quad (6)$$

As shown in the left panel of Fig. 1, in the case of large aspect ratio and weak shaping, the two highly different solvers give almost the same results, and the turbulence dynamics is not sensitive to i) how we solve gyrokinetic Poisson equation. Also carried out are other sensitivity tests. Indeed nonlinear turbulence dynamics is shown to be insensitive to ii) how the simulation mesh is set up (middle panel of Fig. 1) and iii) the number of simulation particles (right panel of Fig. 1). Therefore, the turbulence evolution process, appearing robustly, is not an artificial picture, but real physics. This is important, as a large inward toroidal momentum flux, to be presented, driven with ITG turbulence, is closely related to the transient phase of global turbulence development.

Global gyrokinetic turbulence and driven fluxes are typically characterized by spatio-temporal bursting behavior in various simulations. As shown in Fig. 2, coherent spatio-temporal bursting structures with radially inward propagation, likely to be non-diffusive, are observed in turbulence intensity, zonal flow and associated heat and toroidal momentum flux. A high frequency component shown in the zonal flow is related to geodesic acoustic oscillations with radially varying frequency dependent on the ion temperature profile. The physics processes driving these radially propagating bursting fluctuations may involve turbulence spreading, turbulence and zonal

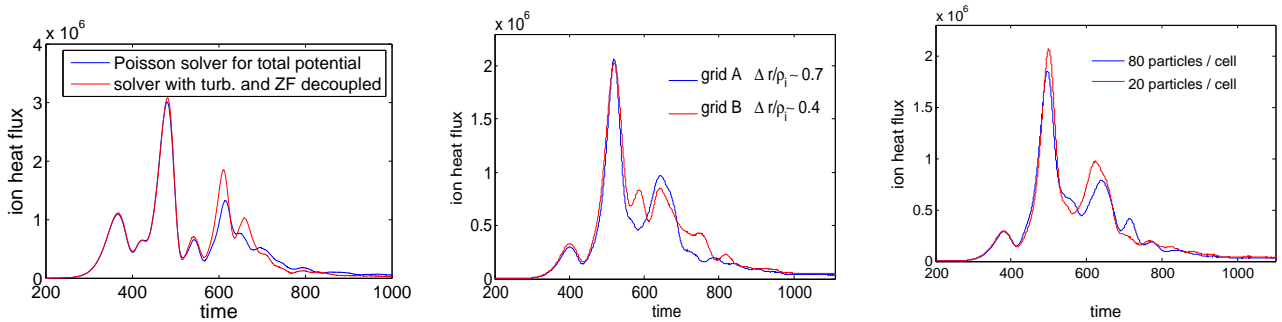


Figure 1: Time evolution of turbulence driven ion heat flux under various numerical sensitivity tests, showing that turbulence dynamics in global simulations is rather robust.

flow interplay, change of local plasma gradients due to turbulence driven transport, etc. The underlying nonlinear physics, however, has not been seriously studied. Its connection with the nature of turbulence transport also needs to be understood.

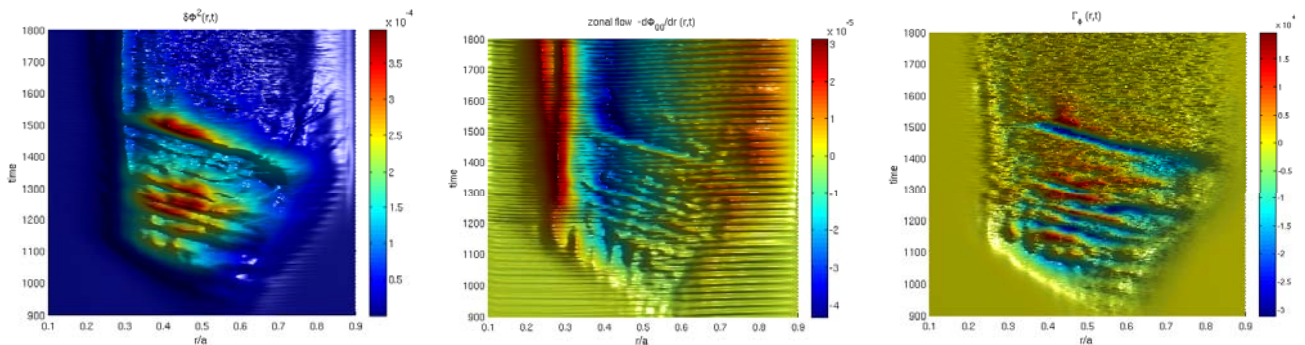


Figure 2: Spatio-temporal evolution of turbulence intensity, zonal flow and momentum flux.

### III. Turbulence driven inward non-diffusive momentum flux and zonal flow shear generated residual stress

The turbulence driven toroidal angular momentum flux in the radial direction, which is defined in general geometry as

$$\langle \vec{\Gamma}_\phi \cdot \hat{\rho} \rangle \equiv \langle \int d^3v m R v_\phi \vec{v}_{\delta E} \cdot \nabla \rho / |\nabla \rho| \delta f \rangle \equiv -m n \chi_\phi^{eff}(\rho) \langle R^2 |\nabla \rho| \rangle \frac{d\omega_\phi}{d\rho}, \quad (7)$$

includes various elements, namely diffusion, convection or “pinch” and off-diagonal flux or fluctuation driven residual stress. A generic structure of toroidal momentum transport was described recently.<sup>7</sup> Searching for nondiffusion elements and understanding underlying mechanisms have been the focus of recently intensive theoretical and experimental effort. A key result of our simulations is the finding of an inward flux of toroidal momentum driven in the post saturation phase of ITG turbulence. Simulation results for a counter-rotating plasma are presented in Fig. 3. where the momentum diffusion is in the inward direction. It is observed that a remarkably large inward toroidal momentum flux occurs during the transient phase of turbulence development, which is after the nonlinear saturation of the ITG instability, but before a well developed steady state. As we discussed before, the appearance of this post-saturation phase flux does not depend on the details of numerical techniques. This inward momentum flux pumps the toroidal momentum from the outer region to the core while maintaining approximately global momentum conservation, resulting in a change in the toroidal rotation with a magnitude of a few percent of the local thermal velocity. Other interesting observations include that the ITG driven momentum

flux settles down to a relatively low level in the long time steady state. Our simulations verify that there exists strong coupling between ITG driven ion momentum and heat transport, and that the ratio of effective momentum and heat diffusivities  $\chi_\phi/\chi_i$  is on the order of unity, as seen in Fig. 3. This is in broad agreement with experimental observations in conventional tokamaks, where low-k fluctuations are believed to be responsible for a high level of plasma transport.<sup>8</sup>

More surprisingly, an inward momentum flux is driven for the case of positive rotation gradient, where the momentum diffusion is outward. This indicates its non-diffusive nature. As a consequence, core plasma rotation spins up, resulting in  $\Delta u_{\parallel}$  a few percent of  $v_{th}$  in the case of no momentum source at the edge. Generally, there are two different channels which contribute to the non-diffusive momentum flux. One is a momentum pinch or convective flux which is proportional to the toroidal rotation velocity; Another is the off-diagonal flux which is driven by residual stress with no dependence on rotation or rotation gradient. Recently extensive theoretical works have been carried out to calculate momentum pinch velocity<sup>9,10</sup> and the residual stress driven by fluctuations and pressure gradients<sup>11</sup>. Identification of various nondiffusive elements and their significance are certainly highly interesting, but difficult in experiments. To this end, we have carried out a series of numerical experiments, with and without mean  $\mathbf{E} \times \mathbf{B}$  shear flow, and with and without toroidal rotation as well as rotation shear. The inward momentum flux is robustly observed in various situations, and appears to be dominated by off-diagonal contributions. It is reasonably anticipated that this off-diagonal flux may lead to the buildup of an experimentally relevant rotation profile structure (i.e., core rotation spin up) when there is a momentum source at the edge; but a true demonstration may require an edge momentum source to be implemented in future simulations on the transport time scale. Moreover, the facts that the long-time steady state toroidal momentum flows against the rotation gradient and that the momentum flux vanishes in cases of rigid rotation (including zero rotation) indicates that it is mostly diffusive.

To obtain a nondiffusive momentum flux, it commonly requires a mechanism for broken  $k_{\parallel}$  spectrum symmetry so as to generate a net acceleration of parallel flow. Such a mechanism includes a mean  $\mathbf{E} \times \mathbf{B}$  velocity shear,<sup>11</sup> which shifts the eigenmode to one side radially, and then producing a non-vanishing averaged  $k_{\parallel}$ . In toroidal geometry, the interplay of magnetic field curvature coupling and ballooning structure is found to cause the symmetry breaking.<sup>9</sup> From the view point of local analysis and simulation, the turbulence self-generated zonal flow shear has no preferred direction in a statistical sense, and therefore has little direct effect. However, for global simulations zonal flow dynamics is found to be significantly different from the local picture. In global ITG turbulence zonal flow is shown to be slowly varying in time and of large

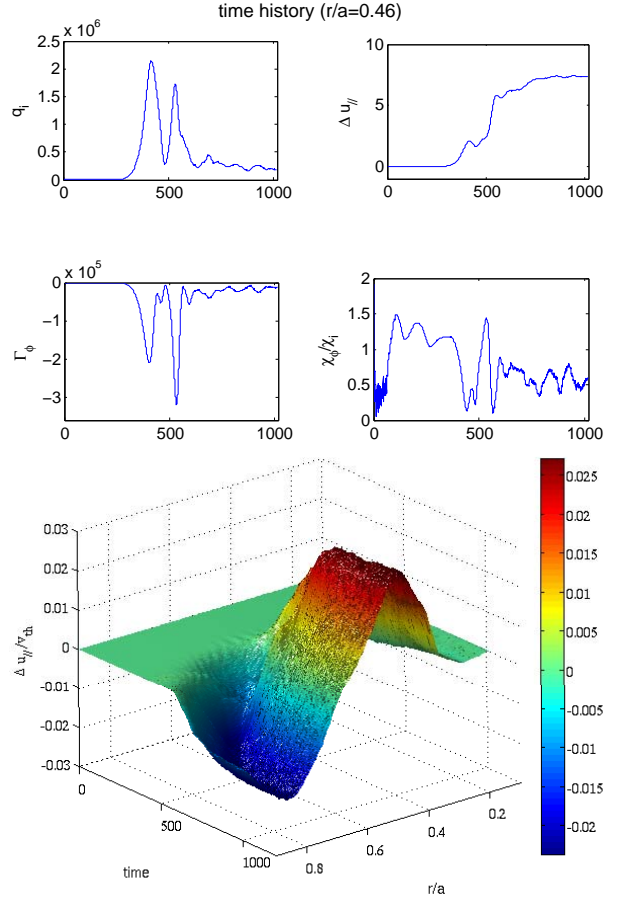


Figure 3: Time history of ion heat flux, parallel velocity, toroidal momentum flux and effective  $\chi_\phi/\chi_i$ , and spatio-temporal evolution of ion parallel flow during ITG turbulence.

scale in space,<sup>2</sup>, as shown in the lower-right panel of Fig. 4. This observation of quasi-stationary zonal flow motivated us to explore the effect of zonal flow shear on  $k_{\parallel}$  symmetry breaking, and has led to the discovery of residual stress generation due to zonal flow shear. The major results are presented in Fig. 4, where the average parallel wavenumber of the turbulence spectrum is defined as

$$\langle k_{\parallel} \rangle(r) \equiv \frac{1}{qR_0} \frac{\sum (nq - m) \delta\Phi_{mn}^2}{\sum \delta\Phi_{mn}^2}. \quad (8)$$

First, the upper left panel shows a close correlation between the toroidal momentum flux  $\Gamma_{\phi}$  and

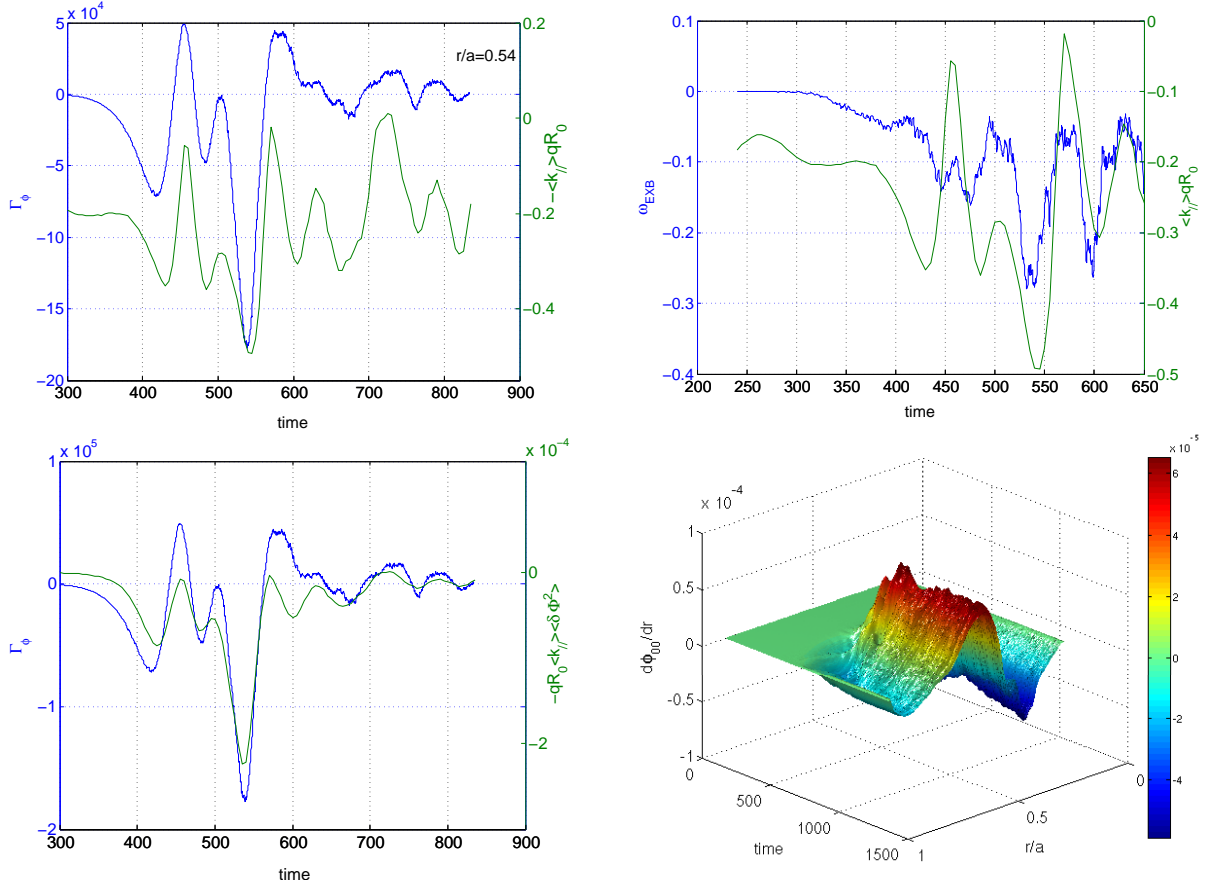


Figure 4: Time history of  $\Gamma_{\phi}$  and  $-\langle k_{\parallel} \rangle$  (upper-left),  $\Gamma_{\phi}$  and  $-\langle k_{\parallel} \rangle \delta\Phi^2$  (lower-left) and zonal flow  $\omega_{E \times B}$  and  $-\langle k_{\parallel} \rangle$  (upper-right); spatio-temporal evolution of zonal flow (lower-right).

$\langle k_{\parallel} \rangle$  in time history. Further, the lower-left panel, showing roughly that  $\Gamma_{\phi} \propto -\langle k_{\parallel} \rangle \delta\Phi^2$ , suggests that the residual stress is a dominant contribution to the inward momentum flux. Finally, a clear correlation between the zonal flow shearing rate  $\omega_{E \times B}$  and  $\langle k_{\parallel} \rangle$  illustrated in the upper-right panel indicates that the non-vanishing  $\langle k_{\parallel} \rangle$  is caused by the zonal flow shear. Therefore the underlying physics for the inward flux is identified to be the generation of residual stress due to  $k_{\parallel}$  symmetry breaking induced by self-generated zonal flow shear, which is quasi-stationary in global simulations. Since zonal flows are nonlinearly self-generated by turbulence, this may represent an universal mechanism to drive a nondiffusive momentum flux via associated residual stress in low- $k$  turbulence. The importance of nondiffusive momentum flux associated with residual stress is emphasized in accounting for the build-up of core peaked rotation profiles in experiments through spontaneous rotation coupled to a dynamic source at the edge.<sup>12</sup>

#### IV. Neoclassical diffusive and non-diffusive momentum flux

An accurate assessment of the baseline of momentum transport due to collisional dissipation

in realistic toroidal plasmas is certainly required to understand any anomalous momentum

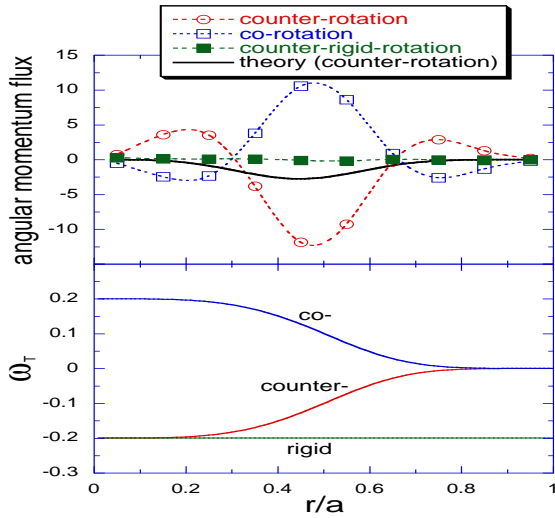


Figure 5: Neoclassical toroidal momentum fluxes from GTC-NEO simulations and theory, showing the enhancement of momentum at steep rotation gradient.

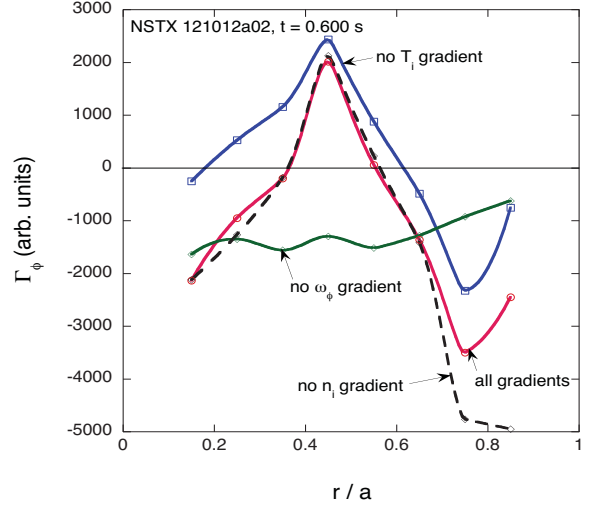


Figure 6: Neoclassical toroidal momentum fluxes vs  $r/a$  from GTC-NEO simulations with various plasma gradients, showing inward momentum flux driven by temperature gradient.

transport and torque in experiments. It is also highly interesting to study nonlocal physics in neoclassical momentum transport and to identify any non-diffusive neoclassical momentum flux. Our global neoclassical particle simulation using the GTC-NEO code, which includes nonlocal physics due to large orbit effects, is employed for these studies. First, it is observed that neoclassical momentum transport in the banana-plateau regime is significantly enhanced when the toroidal rotation gradient is large. In these simulations, off-diagonal flux is excluded by using a uniform temperature profile. As shown in Fig. 5, the simulated neoclassical angular momentum flux in the steep gradient region is 5-6 times larger than the theory prediction.<sup>5</sup> Second, our neoclassical simulations also show that the ion temperature gradient can drive a significant inward nondiffusive momentum flux (Fig. 6). However, the overall neoclassical contribution to the momentum transport is negligibly small compared to experimental levels for NSTX (Fig. 7) and DIII-D plasmas. The effective neoclassical  $\chi_\phi/\chi_i$  is  $\sim 0.1 - 0.01$ , even with the enhancement of momentum transport in the steep rotation profile region.

## V. Residual turbulence and co-existence of normal ion heat and anomalous momentum transport

In general, momentum transport is mostly anomalous even when ion heat transport is reduced to a neoclassical level. The co-existence of normal ion heat and anomalous momentum transport has been widely observed in various machines, but with little understanding. An example is shown in Fig. 7. Motivated by this observation, we have investigate residual low-k turbulence in the regime

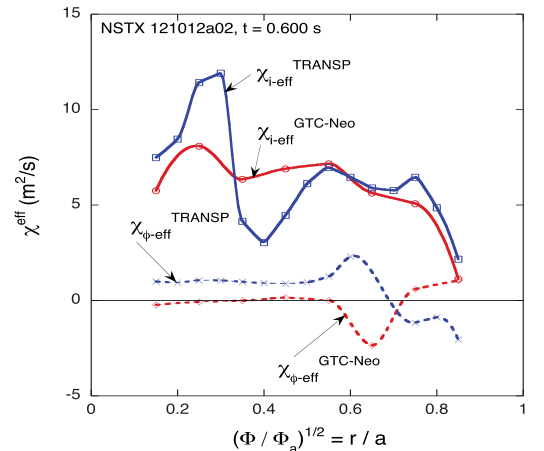


Figure 7: Comparison of GTC-NEO and TRANSP results for effective momentum and heat diffusivity.

of strong  $\mathbf{E} \times \mathbf{B}$  shear. Based on our systematic investigations for both ITG turbulence-driven and neoclassical momentum and heat transport, we propose a possible explanation for this long standing puzzle. First, as is verified by our turbulence simulations, there exists strong coupling between ion momentum and heat transport with the effective  $\chi_\phi/\chi_i$  on the order of unity for ITG turbulence, which is much larger than its neoclassical counterpart. Further, it is found that finite residual turbulence can survive strong mean  $\mathbf{E} \times \mathbf{B}$  shear flow induced damping. As illustrated

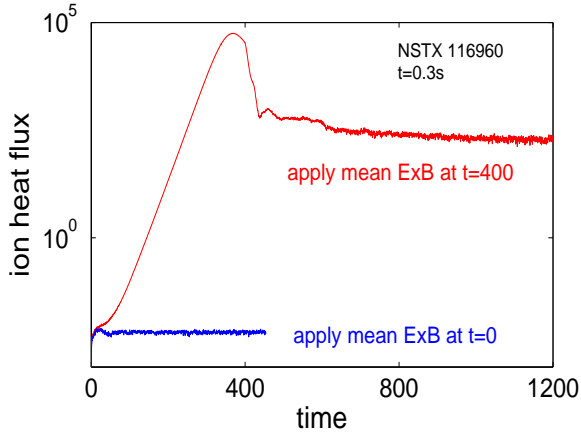


Figure 8: Time history of ion heat flux, showing that residual turbulence survives and drives finite transport.

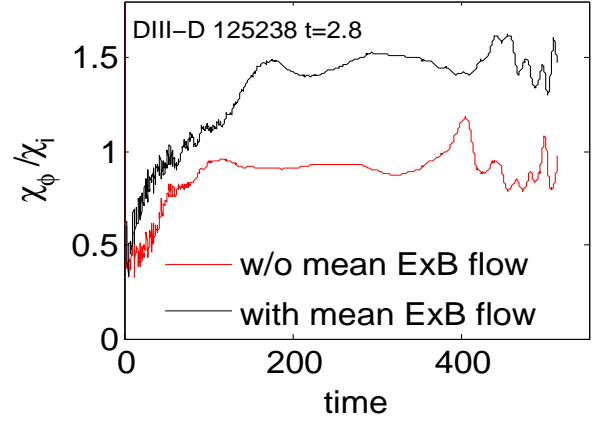


Figure 9: Time history of effective  $\chi_\phi/\chi_i$  from ITG turbulence simulations with and without equilibrium  $\mathbf{E} \times \mathbf{B}$  shear flows for a DIII-D discharge.

in Fig. 8, the ITG instability is shown to be linearly *stable* in the presence of the  $\mathbf{E} \times \mathbf{B}$  shear. However, if we run simulations without the  $\mathbf{E} \times \mathbf{B}$  shear at first, and impose the  $\mathbf{E} \times \mathbf{B}$  shear after the turbulence saturates nonlinearly, we observe that the turbulence, while significantly reduced (by a factor of 10 in intensity), is *not* totally quenched. Results indicate that applying the  $\mathbf{E} \times \mathbf{B}$  shear later (rather than initially) produces results closer to the experimental trends, and the resulting ion heat flux (reduced by a factor of 10) corresponds reasonably closely to the neoclassical value, while the momentum flux remains anomalous, significantly higher than the neoclassical level. Moreover, the effective  $\chi_\phi/\chi_i$  is found to increase in the presence of consistent equilibrium  $\mathbf{E} \times \mathbf{B}$  shear flows, as is shown in Fig. 9. This result indicates that the  $\mathbf{E} \times \mathbf{B}$  flow shear, while lowering all associated turbulence driven radial fluxes via suppressing fluctuations, reduces the transport of energy more efficiently than of momentum. The underlying physics may be related to the generation of residual stress due to the mean  $\mathbf{E} \times \mathbf{B}$  shear induced  $k_{\parallel}$ -symmetry breaking. These findings may offer one explanation for recent experimental observations that the toroidal momentum transport remains highly anomalous, even while the ion heat flux is reduced to a neoclassical level.

## References

- [1] J. E. Rice *et al.*, Nucl. Fusion **44**, 379 (2004).
- [2] W. X. Wang *et al.*, Phys. Plasmas **13**, 092505 (2006).
- [3] S. M. Kaye *et al.*, Nucl. Fusion **47**, 499 (2007).
- [4] W. X. Wang *et al.*, Phys. Plasmas **13**, 082501 (2006).

- [5] F. L. Hinton and S. K. Wong, *Phys. Fluids* **28**, 3028 (1985).
- [6] W. X. Wang *et al.*, *Phys. Plasmas* **14**, 072306 (2007).
- [7] P. H. Diamond *et al.*, *Phys. Plasmas* **15**, 012303 (2008).
- [8] N. Mattor and P. H. Diamond, *Phys. Fluids* **31**, 1180 (1988).
- [9] T. S. Hahm *et al.*, *Phys. Plasmas* **14**, 072302 (2007).
- [10] A. G. Peeters *et al.*, *Phys. Rev. Lett.* **98**, 265003 (2007).
- [11] O. D. Gurcan *et al.*, *Phys. Plasmas* **14**, 042306 (2007).
- [12] P. H. Diamond *et al.*, “Physics of Nondiffusive Turbulent Transport of Momentum and the Origins of Spontaneous Rotation in Tokamaks”, at this IAEA FEC (2008).

This work was supported by U.S. DOE Contract No. DE-AC02-76-CH03073 and the SciDAC project for Gyrokinetic Particle Simulation of Turbulent Transport in Burning Plasmas.